ISSN: 2454-9940

INTERNATIONAL JOURNAL OF APPLIED SCIENCE ENGINEERING AND MANAGEMENT

E-Mail :
editor.ijasem@gmail.com
editor@ijasem.org

www.ijasem.org

INTERNATIONAL JOURNAL OF APPLIED SCIENCE ENGINEERING AND MANAGEMENT

ISSN 2454-9940

www.ijasem.org

Vol 19, Issue 2, 2025

Artificial Neural Network-Based Intelligent Power Switching for Solar-Driven LVDC Nano-Grids

[1]S. Imran Khan, [2]Angadi Haleema Sadiya, [3]Kutagula Shaik Mohammed Ashur, [4] Hanuma Maheshkumar Naik, [5] Neeluri Tharun, [6]Veerapuneni Ganesh,

[2,3,4,5,6] Student,Department of EEE, Ananthalakshmi Institute of Technology and Sciences, Itikalapalli, Near Sk University, Ananthapur.

[1] Assistant Professor, Department of EEE, Ananthalakshmi Institute of Technology and Sciences, Itikalapalli, Near Sk University, Ananthapur.

ABSTRACT

Electricity for remote rural communities, city homes, and the larger grid might soon be within reach with the help of a Low Voltage Direct Current (LVDC) nano-grid. The Power-Sharing Control (PSC) of a solar photovoltaic (PV) system linked to a low-voltage DC nano-grid is presented and studied in this paper. Presented here is a proposed LVDC nano-grid system that makes use of a PSC algorithm executed on a Field Programmable Gate Array (FPGA) to efficiently manage power and control among its many components. The suggested controller is used to analyze the system's performance in general simulation examinations. We build and evaluate the hardware of the planned LVDC nano-grid. We display and discuss the hardware's outcomes under various conditions. Results were obtained via simulation tests using the suggested nano-grid model, which is implemented in matrix laboratory (MATLAB)-Simulink) and has an FPGA-based Maximum Power Point Tracking (MPPT) controller and a central PSC algorithm. Everything is ready to go with the 100 W nano-grid gear. The suggested controller's LVDC nano-grid is analyzed quantitatively in terms of costs and benefits. COLLECTION TERMS: FPGA controller, low voltage DC, nano-grid, renewable energy, solar photovoltaics, DC-DC converter.

INTRODUCTION

New York City's Direct Current (DC) power plant was created by Thomas Edison in 1882. George Westinghouse installed AC distribution in New York City later in 1886. In 1895, after a long and contentious debate among Edison, Tesla, and Westinghouse over how to standardize the Power System (PS) for Energy Consumption (EC), AC Electrical Energy (EE) was finally accepted as the transmission standard [1]. Ever since then, alternating current (AC) has been the main form of power production, transmission, and distribution (DS). Despite EE's existence for over a century, there are still individuals on every continent who do not have access to it. Goal 7 of the Sustainable Development Agenda aims to ensure that all people have access to clean energy. The 2020 SDG7 study states that 770 million people throughout the globe still do not have access to EE. Sub-Saharan Africa has an extremely low electrification rate of about 45%, when compared to the global average. Approximately 580 million people, or over 75% of the world's population, lacked access to EE in 2019. This figure is attributed to the Sub-Saharan area. The coronavirus disease-19 (COVID-19) pandemic has broken the graph, even though there has been great progress in supplying electricity to Sub-Saharan Africa during the last decade. Despite the energy crisis, experts project that 560 million people will live in Sub-Saharan Africa in 2030 [2]. To get beyond the transmission losses in the AC transmission system, the transmission system has already switched to HVDC transmission, which is more technically advanced. When compared to the AC transmission system, the HVDC system provides much higher-quality electricity at a lower cost. The PTAA precursor film had a concentration of 0.5 mM, was spin-coated onto a substrate, and had a depth of less than 1 nm. It is expected that investment would be driven by the fact that solar PV is becoming the low-cost choice for new EE generation globally. Solar photovoltaic (PV) output surpassed 1000 TWh in 2021, an all-time high, thanks to a 22 percent rise. When compared to all other Renewable Energy (RE) technologies, this one has the second-highest absolute generating progress, after wind power [3, 4, 5, 6, 7, 8]. Conversely, DC-powered devices are quickly taking over home and real-time applications because to PS. Multiple conversion steps are necessary because to the traditional DS's AC nature [9], which results in losses and reduces overall efficiency. Just like any other conversion process, there are several steps involved in integrating Renewable Energy Systems (RES) like PV-PS into ACDS. The aforementioned problems have made Low Voltage Direct Current (LVDC) and Direct Current Distribution Systems (DCDS) difficult fields to study. Residential customers in outlying areas without easy or unreliable access to value may have their energy

INTERNATIONAL JOURNAL OF APPLIED SCIENCE ENGINEERING AND MANAGEMENT
ISSN 2454-9940
www.ijasem.org
Vol 19, Issue 2, 2025

requirements met by a DC nano-grid, a low-voltage, low-power DCDS. Electricity in rural regions is now within reach, and the DC nano-grid is opening up new possibilities for electrifying city homes and the cutting-edge Smart Grid (SG) system. AC microgrids are less adaptable than DC nano-grids. The DC nano-grid is able to facilitate the direct integration of DC appliances, such as BLDC fans, LED lamps, and other DC devices. Likewise, there is direct integration of RES, such as solar PV systems with BESS, or battery energy storage systems. Consequently, the several stages of power conversion associated with them are reduced. There are a number of energy quality concerns with DSs and AC transmission, including power, harmonics, reactive power, and frequency synchronization. These issues, however, do not impact DC nano-grids. Direct current nano-grids are easier to handle and regulate than alternating current grids [10]. For the same purposes, DC appliances utilize less power than AC appliances, which reduces the overall EC in addition to the advantages already discussed [11]. As a result, as compared to AC-DSs, DCDS and LVDC models provide better efficiency, reliability, modularity, and cost-effectiveness. With the efficient integration of dispersed generating units, particularly RES, Energy Storage Systems (ESS), and loads, nano-grid will play a crucial role in the future power network [12]. The DC nano-grid, which usually refers to a single residential neighborhood, is a subsystem of the DC micro-grid in the distribution network hierarchy. The DC nano-grid may be run in either an island or grid-connected mode, depending on its design. Various voltage levels (380 v, 48 v, 24 v, 12 v, 400 v, 20 v, 230 v DC, and 325 v DC) have been investigated in relation to the LVDC design and DCDS [13]. numerous publications choose 48 v DC as a standard because it meets numerous criteria that affect the DCDS's performance, including a safe voltage level, storage feasibility, and system efficiency [14]. A thorough introduction to DCDS and the LVDC architecture is given by the author in [15]. The article covers a variety of topics, including LVDC architectural types, DC architecture productivity analysis using voltage levels, LVDC and DC network safety features, and standards that have been put into place globally. The reliability investigation and cost analysis are presented in a comprehensive review and commentary on DC, AC, and hybrid nano-grids [16]. A statistical analysis is used to analyze the real-time cost of hybrid nano-grid Demand Side Management (DSM).

LOW VOLTAGE DIRECT CURRENT NANO GRID SYSTEM

You can see the suggested DC nano-grid system in Figure 1. An LVDC nano-grid's main source is a renewable energy system (RES), while the BESS serves as an external source. The FPGA controller, a bidirectional DC-to-DC converter that connects the battery to the grid, and an MPPT controller are additional essential parts of the grid system. The DC-DC boost converter is used in solar PV systems.

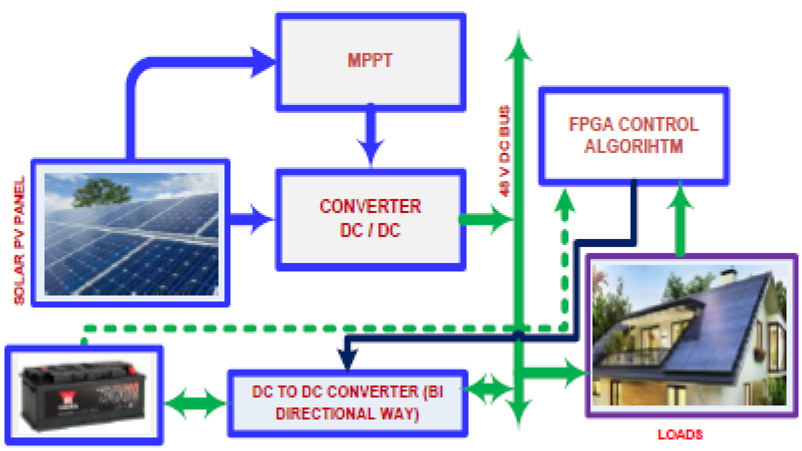

FIGURE 1. LVDC nano-grid with solar PV and BESS

An MPPT controller is often engaged to ensure the efficient functioning of the SPV system due to the intermittent and variable output of the solar PV module. The P&O MPPT algorithm is used for peak power harvesting in this study. For the ESS, a 12 v, 20 Ah battery is used. All of the converters that are linked to the grid are controlled by the FPGA controller, which functions as the main controller. In the FPGA controller, the P&O MPPT algorithm is used. Power availability from the source, energy storage system (ESS), and load power needs determine the grid operating modes. The following sections outline the many possible modes of operation for the LVDC nano-grid. Mode A. In Mode 1, the amount of electricity generated by the solar panels is enough to power the load. Direct current is supplied to the load.

ISSN 2454-9940
www.ijasem.org
Vol 19, Issue 2, 2025

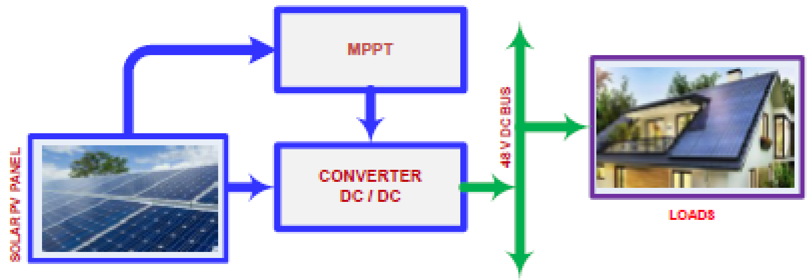

FIGURE 2. Mode 1 Operation

B. MODE 2

Here, the load is thought of as being in a "ON" state. The PV source produces more electricity than the load really needs. Figure 3 shows the process of supplying the load with electricity produced by PV and charging the batteries with the extra energy.

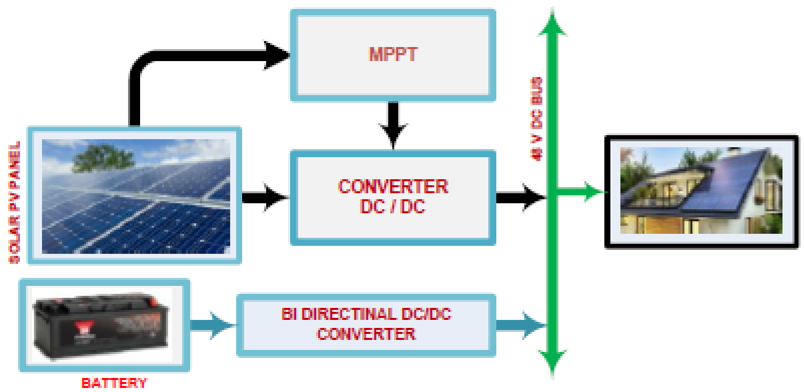

FIGURE 3. Mode 2 Operation

C. MODE 3

Mode 3 makes use of the available PV electricity when the load is disconnected. Charging the batteries consumes all of the electricity produced by the PV system. The DC bus transfers energy from the photovoltaic (PV) source to the battery, as seen in Figure 4.

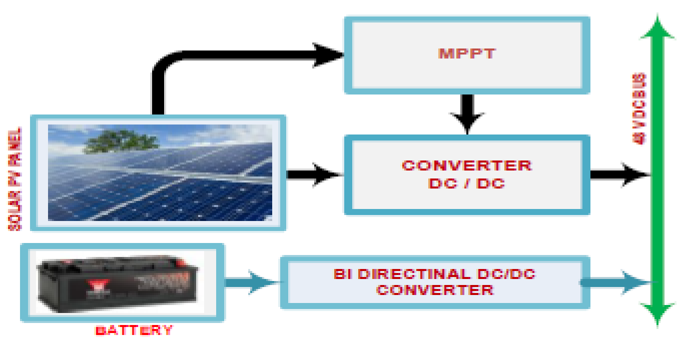

FIGURE 4. Mode 3 Operation

D. MODE 4

It says "ON" here. However, PV power generation falls short of meeting the demand. So, to fulfill the load power need, ESS provides the extra capacity. Figure 5 shows the direction of the power flow.

INTERNATIONAL JOURNAL OF APPLIED SCIENCE ENGINEERING AND MANAGEMENT

ISSN 2454-9940

www.ijasem.org

Vol 19, Issue 2, 2025

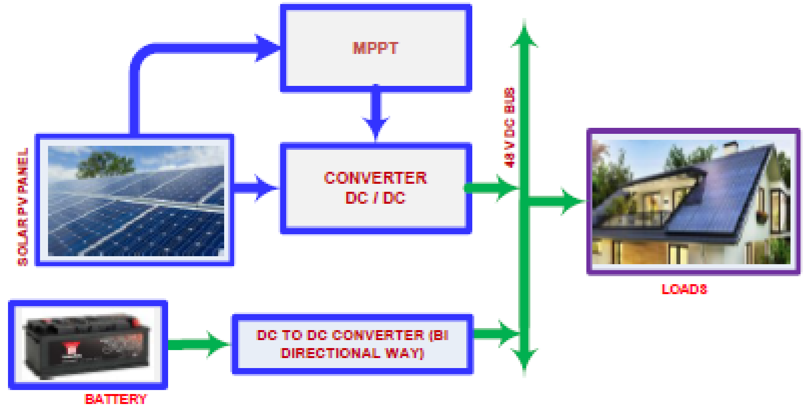

FIGURE 5. Mode 4 Operation

E.MODE 5

Mode 5's load is "ON," but PV power isn't accessible. Figure 6 shows that in this case the load is provided straight from the battery.

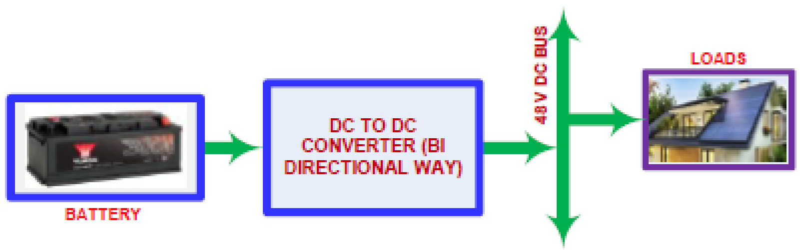

FIGURE 6. Mode 5 Operation

Conditions and limits, including the battery's State of Charge (SoC), determine how to charge and discharge the battery. Throughout all operations, the components of the nano-grid are controlled by the FPGA to ensure that the power-sharing between the source and loads is maintained.

MAXIMUM POWER POINT TRACKING AND POWER-SHARING CONTROL OF LVDC NANO-GRID USING FIELD PROGRAMMABLE GATE ARRAY

The FPGA controller's effectiveness stems from its field-programmable features and ability to operate in parallel. The FPGA controller offers a great deal of leeway in hardware interface design and implementation. Due to the ease of configuring and converting any MATLAB model to a real-time controller, an FPGA may be reprogrammed in any iteration. With the help of the FPGA Spartan 6 controller, the MPPT and PSC algorithms are put into action in the suggested nano-grid system.

INTERNATIONAL JOURNAL OF APPLIED SCIENCE ENGINEERING AND MANAGEMENT

ISSN 2454-9940

www.ijasem.org

Vol 19, Issue 2, 2025

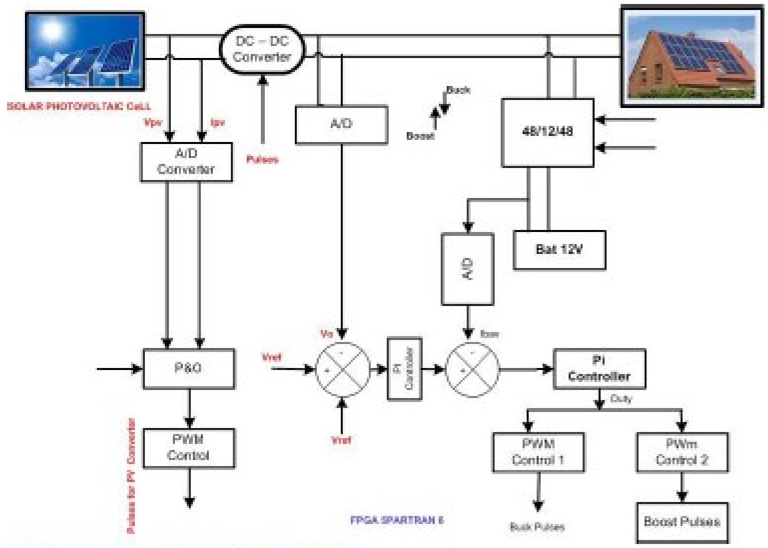

FIGURE 7. Conceptual Diagram

The schematic of an LVDC nano-grid using an FPGA may be shown in Figure 7. Figure: Field-programmable gate array (FPGA) controllers keep an eye on various electrical characteristics throughout the circuit and send out signals to manage the subsystems based on what they find. The primary goal is to regulate the DC bus voltage and the flow of power from sources to loads. In this setup, two separate electronic converters for converting electricity are used. Based on the bus voltage, the bidirectional buck-boost converter linked between the battery and the 48 v DC bus is independently owned, while the MPPT controller controls the DC-DC boost converter attached to the PV source. The bidirectional converter's mode of operation is switched between buck and boost depending on the level of the bus voltage, which the controller continually senses. In order to prevent the system from being damaged by bus overvoltage when there is no load or an open circuit, the bus voltage is set to 50 volts, which is the saturation level [24, 25, 26].

Tracking Algorithm for Maximum Power Points

Irradiation and temperature are two environmental factors that affect how much electricity solar PV modules can generate. A solar PV module's output voltage or current fluctuates in response to changes in environmental circumstances, leading to variations in the power provided by the module. According to Figure 8, a standard 50 Wp PV module's PV characteristics are shown for various input situations. The graphic clearly shows that as the temperature or sun irradiation varies, the maximum power produced by the PV modules also fluctuates. As the physical or electrical factors of the PV module change, the operating point of the converter is fine-tuned using the maximum power point tracking algorithm. In this manner, the maximum power point tracking (MPPT) controller guarantees that the solar PV system operates at its greatest capacity and achieves maximum power production under all conditions.

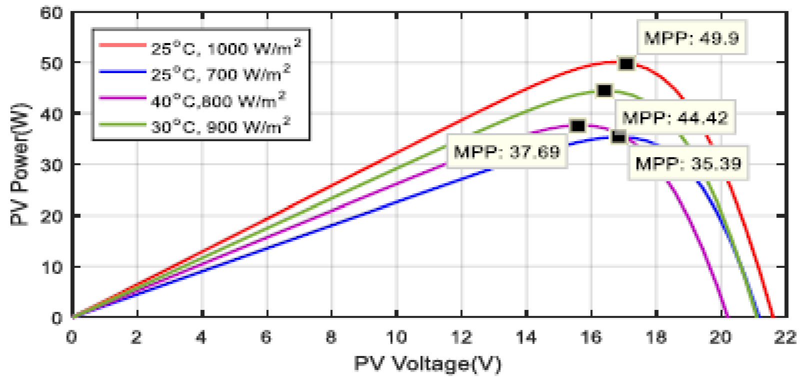

FIGURE 8. Power-voltage characteristics of PV with multiple input

Various forms of literature provide various strategies for MPP tracking. When compared to other traditional algorithms, the Perturb & Observe (P&O) technique has the highest level of acceptance among MPPT methods. The simplicity and convenience of deployment of the P&O MPPT are its key features. In this study, the P&O MPPT algorithm is used to monitor MPPs. Figure 9 illustrates the process of the P&O algorithm. P&O MPPT achieves MPP by routinely computing the slope and then applying perturbation. Assuming $\nabla \boldsymbol{Ppn\ Vpn}$ is greater than 0, the duty ratio goes up and the perturbation keeps going in the same direction until it reaches MPP. If $\nabla \boldsymbol{Ppn\ Vpn}$ is less than 0, the duty ratio is reduced in stages to achieve MPP, but otherwise, the order of concern is reset. This ensures that the PV module is always operating at its full power output.

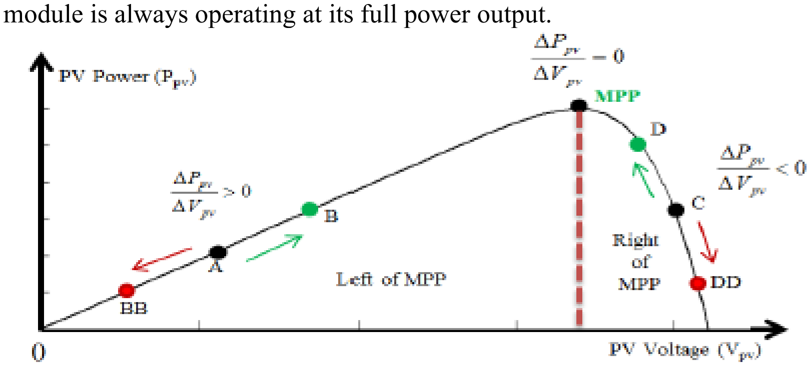

FIGURE 9.Observation and perturbation of P&O MPPT

The flowchart of the P&O MPPT is shown in Figure 10, and Figure 11 represents the P&O MPPT model implemented using the Xlinx Blockset in MATLAB [27].

INTERNATIONAL JOURNAL OF APPLIED SCIENCE ENGINEERING AND MANAGEMENT
ISSN 2454-9940
www.ijasem.org
Vol 19, Issue 2, 2025

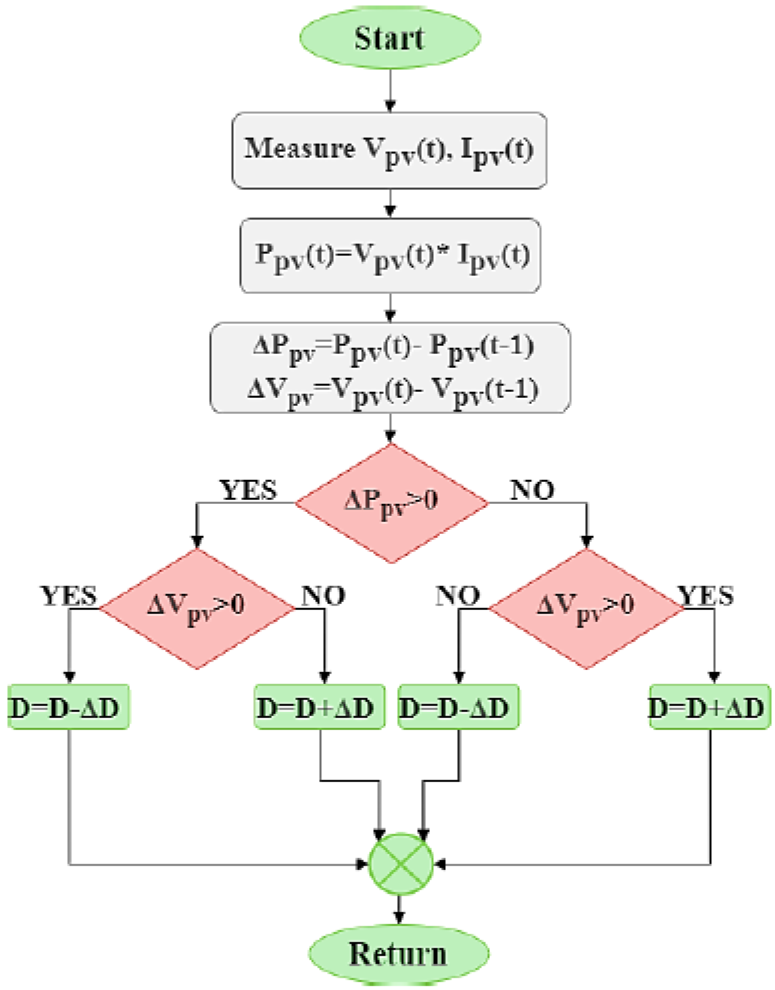

FIGURE 10. P&O MPPT flowchart

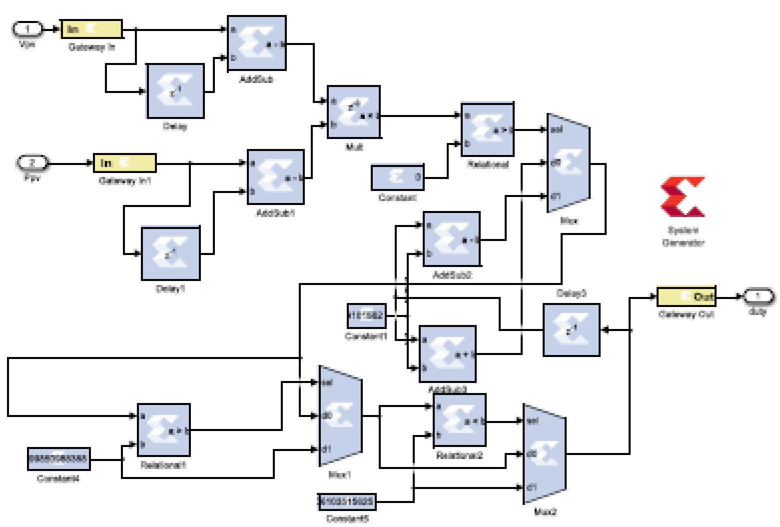

FIGURE 11. FPGA implementation of the P&O algorithm

POWER SHARING CONTROL SYSTEM

Taking into account the following factors: the load's power demand (Pload), the energy accessibility in the energy storage system (ESS), and the power accessible from the solar PV source (Ppv), the suggested control system is constructed utilizing an FPGA controller. Pload>Ppv indicates that the power requirements of the load will be satisfied by PV-generated and ESS power when the load power exceeds the PV-generated power. The battery's state of charge (SoC) must be higher than the specified value in order for this to be met. A minimum of 25% battery SoC is established in this work. If the power provided by the main source is lower than the demand from the load and the state of charge of the battery is less than 25%, the load will be turned off and the excess power will be used to charge the battery. However, the battery unit is charged until the state of charge (SoC) reaches its maximum value if the power provided by the PV source, Ppv, is excessive, as is the load demand, Pload. As illustrated in Figure 4, the proposed system's PSC employs an EMS algorithm that was constructed utilizing an FPGA. The DC bus and the battery storage unit are both integrated by the bidirectional buck-boost converter. In order to provide the necessary power to the grid, the converter operates in boost mode. As a result, ESS is released. In order to provide ESS with the enhanced grid energy, the converter will be operated in buck mode. For optimal power-sharing in every situation, the bidirectional converter's operation may be switched between boost and buck modes by means of the central control algorithm. Figure 8 displays the MATLAB model of the control algorithm that was created using the Xilinx blockset.

Here we go over the planned LVDC nano grid system's power sharing controls. An FPGA controller is used to generate the suggested control strategy, which takes into account the available power from the source, the availability of ESS, and the energy needed by the load. FPGA controllers keep an eye on the circuit's electrical properties at various points and then issue directives to the subsystems based on what they find. The controller used is a Spartan6 FPGA. This section delves into the topic of power sharing control inside the planned LVDC nanogrid technology. The suggested control system takes into account both the energy supply from the source (ESS) and the energy consumption of the load; it is constructed utilizing an FPGA controller. FPGA controllers keep an eye on the circuit's electrical properties at various stages and then issue directives to the subsystems based on what they find. The controller used is a Spartan6 FPGA. Because of their comparable functions and configurable field features, FPGA controllers are beneficial. Because any model generated in MATLAB can be quickly converted to a real-time controller, the FPGA controller offers a great deal of hardware interfacing freedom when it comes to controller design and implementation. To add, the chip is reprogrammed in an FPGA. This approach turns into a sizable logic circuit set up in accordance with a design; nevertheless, if modifications are necessary, it is updated by reprogramming it for each repetition. In order to account for the ESS, we rewrite the power balancing equation (EQU) (1) as EQU (2) and EQU (3) for the first case.

$$P_{pv} = P_{total} + P_{ESS} \quad (1)$$

$$P_{net} = P_{Load} - P_{pv} \quad (2)$$

$$P_{net} + P_{pv} = P_{Load} \text{ when } P_{pv} \leq P_{Load} \text{ and } SOC_{ESS} \rangle 20\% \quad (3)$$

The primary goal is to regulate the DC bus voltage and the flow of power from sources to loads. Figure 12 displays the controller's conceptual flow diagram. The component parts are autonomous power electronic converters. Based on the bus voltage, the bidirectional buck-boost converter linked between the battery and the 48 v DC bus is independently owned, while the MPPT controller controls the DC-DC boost converter attached to the PV source.

INTERNATIONAL JOURNAL OF APPLIED SCIENCE ENGINEERING AND MANAGEMENT
ISSN 2454-9940
www.ijasem.org
Vol 19, Issue 2, 2025

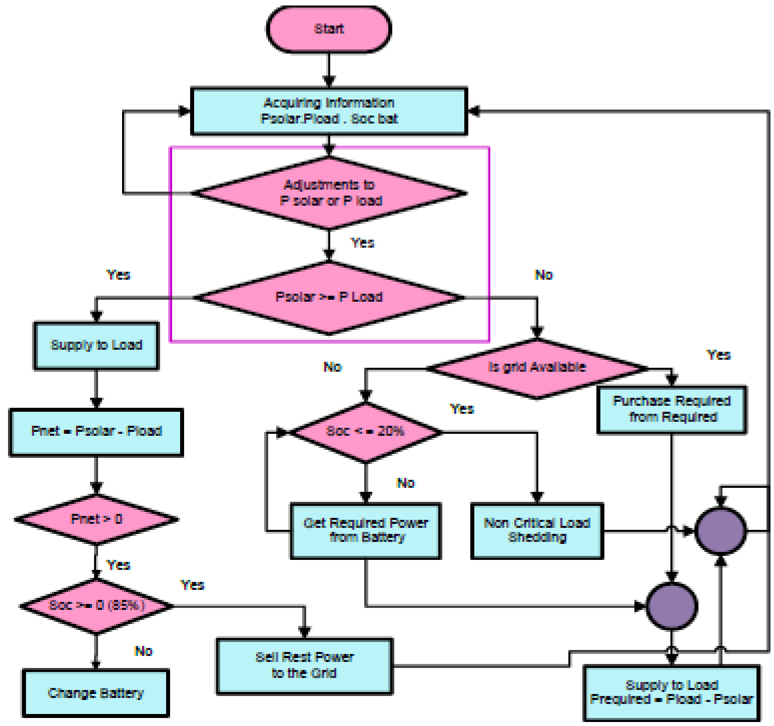

FIGURE 12. Power sharing control algorithm for LV nano grid

SIMULATION AND ANALYSIS

Using MATLAB/Simulink, we constructed an LVDC nano-grid model with 100 Wp of solar PV production and a 200 W maximum load. The converter circuits used in this project adhere to the established protocols for design. The bidirectional Buck-Boost converter, PV module, and boost converter specs are shown in the table. Discrete input circumstances are used to test the simulation research. In the first scenario, the load changes every 100 milliseconds while the solar PV production remains constant. In Figure 13 (a), we can see the PV-generated, load, and battery power. In Figure 13 (c), we can see the battery system-on-a-chip, the Boost converter, and the Buck converter in their respective switching states. Where generation and load demand fluctuate continually is determined by the simulation research. Here, there is a 100 ms interval between changes in PV production and load demand. Figures 13 (a) and 13 (b) show the simulation results for the chosen themes.

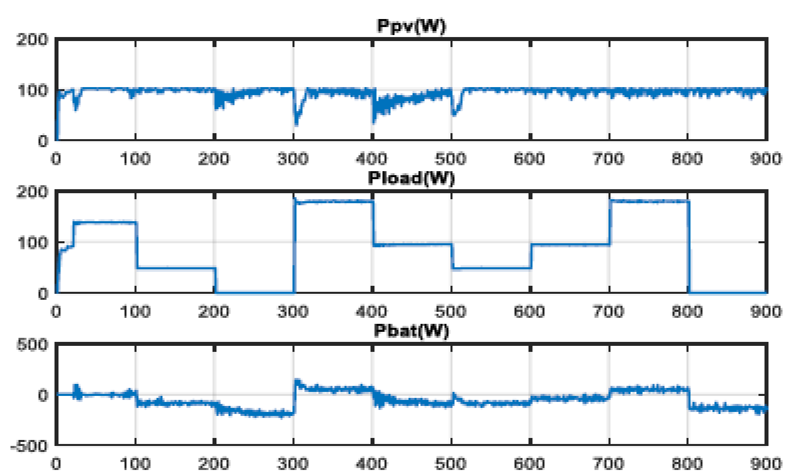

FIGURE 13 (a). Power generated by PV, power flow in ESS, load demand

INTERNATIONAL JOURNAL OF APPLIED SCIENCE ENGINEERING AND MANAGEMENT

ISSN 2454-9940

www.ijasem.org

Vol 19, Issue 2, 2025

According to the data, the suggested controller successfully toggles the bidirectional converter between boost and buck modes to keep power flowing to the source, load, and ESS. At 500 ms, for instance, the load power in the first case abruptly decreased to almost 50% of the operational load. It led to a precipitous decline in solar PV output, as seen in Figure 13 (a). In response to the change, the controller immediately activates the bidirectional converter, causing it to run in boost mode and drain the battery to satisfy the load power requirements. Concurrently, however, P&O MPPT initiated the disruption in order to maximize the performance of the solar PV system. Figure 13 (b) shows that as a result, solar PV production has begun to rise, and that the bidirectional converter enters battery charging (boost) mode when PV generation surpasses the load requirement. In Case 2, at 100 ms, the same thing happens. At 100 ms, the load power went to zero, and PV production decreased, as shown in Figure 14 (a). The controller took the load power from the previous interval into account when it switched the ESS converter to deliver battery power to the load when generation fell. Figure 14 (b) shows that the algorithm returned the converter to buck mode in order to charge the battery after it recognized the load power was zero and PV produced some capacity. The abrupt rise in load impacts the generator at 500 ms. However, in this case as well, the P&O MPPT initiated the disturbance in order to run the PV system and achieve high energy, and the system has now returned to its real operational position. The dependability, speed, and precision of this suggested controller are confirmed by the reported results and the discussion.

TABLE I. SOLAR PANELS, BATTERIES, AND INVERTER INVESTMENT IN CASE III

Device	Power	Cost	Units	Total Cost
Solar Panel	340 W	350 $	882	308700 $
Solar Inverter	50 kV	6987 $	5	42000 $
Solar Batteries				
School	150 Ah	256.24 $	9	2304 $
Post Office	150 Ah	256.24 $	3	768 $
Panchayat Office	100 Ah	215.00 $	6	1290 $
				355062 $

TABLE II. SOLAR PANELS, BATTERIES, AND INVERTER INVESTMENT IN CASE II

Residential Area				
Device	Power Unit	Cost	Units	Total Cost
Solar Array	900 W	630 $	500	315000 $ in to rupee
Solar Inverter	250 VA	78 $	500	3900 $
Solar Batteries	60 Ah	60 $	1500	90000 $
				408900 $

Case 1: This section will include the overall cost analysis of all devices used in the grid setup for EE generation. In Table 3 we can see the whole cost of putting up Case 1. Case 2: This section delves into the comprehensive cost analysis of all the components used in the establishment of an off-grid battery backup system for producing EE and storing energy. In Table 2 you can see the whole amount needed to set up Case 2. In the third case, we looked at the overall system units, their costs, and the power consumption of each unit.

TABLE III. SOLAR PANELS, BATTERIES, AND INVERTER INVESTMENT IN CASE I

Device	Power	Cost	Units	Total Cost
Solar Panel	340 W	350$	882	308700 $
Inverter	10 kV	1218$	30	36540 $
			Total Cost	345240 $

COST ANALYSIS OF LIGHTING & VENTILATION WITH POWER FLOW CONTROLLER

ISSN 2454-9940
www.ijasem.org
Vol 19, Issue 2, 2025

At subsidised prices, the government is distributing and supplying 9 W LED lights and 20 W tube lights for the village's lighting and ventilation needs. Additionally, they are subsidizing a 70 W ceiling fan for the same reason. You may pay for this project in installments via your monthly power bills. It comes with two LED lamps and one tube light for the home sector. In this section, we examine the rural regions' economies.

TABLE IV. LIGHTING AND VENTILATION INVESTMENT IN THE RESIDENTIAL SECTOR

Device	Power	Cost	Units	Total Cost
LED Bulb	9 W	1.09 $	2	2.18 $
LED Tube Light	20 W	3.53 $	1	3.53 $
Fan	70 W	15.30 $	1	15.30 $
Total				21 $
For 500 Houses				10500 $

The overall cost for lighting and ventilation would be uniform while computing the overall project cost for I, II, and III.

CONCLUSION

Using a Field Programmable Gate Array (FPGA) controller, this research proposes a Low Voltage Direct Current (LVDC) nano-grid. A thorough evaluation of the suggested nano-grid was put to the test using a combination of software and hardware implementation. Results were obtained via simulation experiments done under varied Cases using the suggested nano-grid model, which includes a central control algorithm for power-sharing and an FPGA-based Maximum Power Point Tracking (MPPT) controller. The model was created in MATLAB. Additionally, the 100 W nano-grid's hardware configuration has been accomplished and verified. By doing a full cost analysis using the suggested controller for several case studies, we can examine the nano-grid system's cost-effectiveness.

REFERENCES

[1] Chen, Yandong, Yang Jie, Jiaqing Zhu, Qixin Lu, Yu Cheng, Xia Cao, and Zhong Lin Wang, "Hybridized triboelectric-electromagnetic nanogenerators and solar cell for energy harvesting and wireless power transmission." *Nano Research*, 15, no. 3, pp. 2069-2076, 2022.

[2] Mohsan, Syed Agha Hassnain, Muhammad Asghar Khan, Alireza Mazinani, Mohammed H. Alsharif, and Ho-Shin Cho. "Enabling Underwater Wireless Power Transfer towards Sixth Generation (6G) Wireless Networks: Opportunities, Recent Advances, and Technical Challenges." *Journal of Marine Science and Engineering*," no. 9,2022.

[3] Muthuvel, Periyasamy, S. Arul Daniel, and Sajal K. Paul. "Sizing of PV array in a DC nano-grid for isolated households after alteration in time of consumption." *Engineering Science and Technology, an International Journal*", vol. 20, pp. 1632-1641,2017.

[4] Ming Wang, Huaxin Wang, Wei Li, Xiaofei Hu, Kuan Sun, Zhigang Zang, "Defect passivation using ultrathin PTAA layers for efficient and stable perovskite solar cells with a high fill factor and eliminated hysteresis," *J. Mater. Chem. A*, 2019, vol. 7, pp. 26421-26428 https://doi.org/10.1039/C9TA08314F

[5] Yanfeng Miao, Xingtao Wang, Haijuan Zhang, Taiyang Zhanga, Ning Wei, Xiaomin Liu, Yuetian Chen, Jie Chen, Yixin Zhao, "In situ growth of ultra-thin perovskitoid layer to stabilize and passivate MAPbI3 for efficient and stable photovoltaics," *eScience*, vol. 1, 2021, pp. 91–97, https://doi.org/10.1016/j.esci.2021.09.005

[6] Yiyi Zhu, Lei Shu, Qianpeng Zhang, Yudong Zhu, Swapnadeep Poddar, Chen Wang, Zhubing He, Zhiyong Fan, "Moth eye-inspired highly efficient, robust, and neutral-coloured semitransparent perovskite solar cells for building-integrated photovoltaics," *EcoMat.*, 2021, vol, 3, no. e12117, https://doi.org/10.1002/eom2.12117

[7] Qiang Lou, Huilin Li, Qingsong Huang, Zhitao Shen, Fumin Li, Qing Du, Mengqi Jin, Chong Chen, "Multifunctional CNT: TiO2 additives in spiro-OMeTAD layer for highly efficient and stable perovskite solar cells," *EcoMat*, 2021, vol. 3, no. e12099, https://doi.org/10.1002/eom2.12099.

[8] Binbin Huang, Zemin Sun, Genban Sun, "Recent progress in cathodic reduction-enabled organic electrosynthesis: Trends, challenges, and opportunities," *eScience*, vol. 2, 2022, pp. 243–277, https://doi.org/10.1016/j.esci.2022.04.006

[9] M. A. Shamshuddin, S. B Thanikanti, V. K. Ramachandaramurthy, & R. Kennel, “Implementation and design of an autonomous residential DC nano grid”, *In PCIM Europe 2019; International Exhibition and Conference for Power Electronics, Intelligent Motion, Renewable Energy and Energy Management*, pp. 1-8, 2019.

[10] Mohamed, Naoui, Flah Aymen, Mohammed Alqarni, Rania A. Turky, Basem Alamri, Ziad M. Ali, and Shady HE Abdel Aleem, "A new wireless charging system for electric vehicles using two receiver coils", *Ain Shams Engineering Journal*, no. 2, 2022.

[11] Mohamed, Naoui, Flah Aymen, Mohammed Alqarni, Rania A. Turky, Basem Alamri, Ziad M. Ali, and Shady HE Abdel Aleem, "A new wireless charging system for electric vehicles using two receiver coils", *Ain Shams Engineering Journal*, vo. 13, no. 2, 2022.

[12] V. A. Prabhala, B.P. Baddipadiga, P. Fajri & M. Ferdowsi, “An overview of direct current distribution system architectures & benefits”, *Energies*, vol. 1, no. 9, 2018.

[13] S. Moussa, M. J. B. Ghorbal & I. S. Belkhodja, “Bus voltage level choice for standalone residential DC nano grid”, *Sustainable Cities and Society*, no. 46, 2019.

[14] Sabry, Ahmad H., Abidaoun H. Shallal, Hayder Salim Hameed, and Pin Jern Ker, “Compatibility of household appliances with DC microgrid for PV systems”, *Heliyon*, vol. 6, no. 12, pp. e07744, 2020.

[15] Ouramdane, Oussama, Elhoussin Elbouchikhi, Yassine Amirat, Franck Le Gall, and Ehsan Sedgh Gooya, "Home Energy Management Considering Renewable Resources, Energy Storage, and an Electric Vehicle as a Backup", *Energies*, vol. 15, no. 8 pp. 2830, 2022, https://doi.org/10.3390/en15082830

[16] K. Siraj and H. Khan, “DC distribution for residential power networks—A framework to analyze the impact of voltage levels on energy efficiency,” *Energy Reports*, no. 6, pp. 944-951, 2020.

[17] D. Burmester, R. Rayudu, W. Seah, D. Akinyele, “A review of nano grid topologies and technologies”, Renewable and sustainable energy reviews, no. 67, pp. 760-775, 2017.

[18] Badar, Altaf QH, and Amjad Anvari-Moghaddam, “Smart home energy management system–a review", *Advances in Building Energy”,* vol. 16, no. 1, pp. 118-143, 2022, https://doi.org/10.1080/17512549.2020.1806925

[19] Mohammad, Arshad, Mohd Zuhaib, and Imtiaz Ashraf, “An optimal home energy management system with integration of renewable energy and energy storage with home to grid capability." *International Journal of Energy Research,* vol. 46, no. 6, pp. 8352-8366, 2022.

[20] Mahapatra, Bandana, and Anand Nayyar, "Home energy management system (HEMS): Concept, architecture, infrastructure, challenges and energy management scheme,” *Energy Systems, vol. 1*3, pp. 643-669, 2022, https://doi.org/10.1007/s12667-019-00364-w